Cell Architecture: Surrounding Muscle Cells Shape Gland Cell Morphology in the *Caenorhabditis elegans* Pharynx

Wahyu Hendrati Raharjo,* Vikas Ghai,*,† Aidan Dineen,*,‡ Michael Bastiani,§ and Jeb Gaudet*,†,1
*Genes and Development Research Group, Alberta Children's Hospital Research Institute for Child and Maternal Health, †Department of Molecular Biology and Biochemistry, and ‡Graduate Program in Medical and Molecular Genetics, University of Calgary, Calgary, Alberta, T2N 4N1, Canada, and §Department of Biology, University of Utah, Salt Lake City, Utah 84112

ABSTRACT The acquisition and maintenance of shape is critical for the normal function of most cells. Here we investigate the morphology of the pharyngeal glands of *Caenorhabditis elegans*. These unicellular glands have long cellular processes that extend discrete lengths through the pharyngeal musculature and terminate at ducts connected to the pharyngeal lumen. From a genetic screen we identified several mutants that affect pharyngeal gland morphology. The most severe such mutant is an allele of *sma-1*, which encodes a β-spectrin required for embryonic elongation, including elongation of the pharynx. In *sma-1* mutants, gland projections form normally but become increasingly abnormal over time, acquiring additional branches, outgrowths, and swelling, suggestive of hypertrophy. Rather than acting in pharyngeal glands, *sma-1* functions in the surrounding musculature, suggesting that pharyngeal muscles play a critical role in maintenance of gland morphology by restricting their growth, and analysis of other mutants known to affect pharyngeal muscles supports this hypothesis. We suggest that gland morphology is maintained by a balance of forces from the muscles and the glands.

ACQUISITION of shape is an important step in the maturation and function of cells, the maxim "form follows function" being as much a principle of biology as in other disciplines. In some cases, morphology is a largely intrinsic property of the cell necessary for function, as for example the biconcave disk shape of mammalian erythrocytes or the capacity of neurons grown in culture to develop axons. In other cases, cell morphology results from interactions between a cell and its surroundings, including other cells and the extracellular matrix (ECM). Such interactions are particularly evident in the formation of complex organ structures, in which a variety of different cell types must interact to form a mature, functioning structure.

The *Caenorhabditis elegans* pharynx serves as a useful model for organ development: morphogenetic events can be analyzed both at the level of the whole organ and at the level of individual cells. The usual advantages of model organism genetics and the transparency of the nematode apply to study of the pharynx, as does the relative simplicity of the organ (95 cells in total) (Mango 2009; Kormish *et al.* 2010). However, the pharynx also exhibits features of more complex organs, in particular, the diverse lineal histories of pharyngeal cells and the presence of multiple different cell types within the organ (Sulston *et al.* 1983). Previous studies have elucidated some aspects of pharyngeal morphogenesis, such as the attachment of the pharynx to the buccal cavity (or mouth) and the intricate formation of two toroid cells (pm8 and vpi1) that connect the pharynx to the intestine (Portereiko and Mango 2001; Rasmussen *et al.* 2008). In the case of pharyngeal attachment, changes in cell shape and orientation at the anterior end of the pharynx lead to epithelial connections that anchor the pharynx to the mouth of the animal; this connection is ultimately required for the proper elongation of the organ as a whole. In **p**harynx **un**attached (Pun) mutants, the organ generally lacks the distinct bilobed shape that results from differential elongation of pharyngeal cells (Fay *et al.* 2004; Qiu and Fay 2006; Mani and Fay 2009). The formation of the pm8 and vpi1 cells at the posterior end of the pharynx is likewise

doi: 10.1534/genetics.111.132449
Manuscript received July 8, 2011; accepted for publication July 30, 2011
Available freely online through the author-supported open access option.
Supporting information is available online at http://www.genetics.org/content/suppl/2011/08/25/genetics.111.132449.DC1.
[1]Corresponding author: Department of Biochemistry and Molecular Biology, 3330 Hospital Dr., NW, Calgary, Alberta, T2N 4N1, Canada. E-mail: gaudetj@ucalgary.ca

a study of cell shape arising from a combination of intrinsic cellular properties and interactions with neighboring cells. Careful analysis of pm8 development revealed a dorsal-to-ventral movement of the cell, akin to a falling curtain, during which movement the cell drapes itself around extensions from a neighboring support cell, the mc3 marginal cell (Rasmussen *et al.* 2008). Following this movement, the cell self-fuses to produce the terminal toroid shape of pm8.

Other cells within the pharynx have unique and interesting morphologies, such as the pharyngeal glands (Albertson and Thomson 1976), which are the focus of this article. The five pharyngeal glands are single-celled structures, whose cell bodies reside in the posterior bulb of the pharynx (Figure 1A). Each of the glands connects to the pharyngeal lumen via a cellular extension that differs in length and connectivity depending on the cell's subtype. The longest projection is made by g1P and extends a distance of ~125 μm in adults, terminating at a duct near the anterior end of the pharynx. The projections of the two g1A cells extend ~50 μm in adults and form ducts at the posterior end of the anterior pharyngeal bulb. Finally, the two g2 cells have relatively short extensions (<10 μm) that connect to the lumen within the posterior bulb. Along their length, these extensions are flanked by pairs of pharyngeal muscle cells that ultimately fuse to form binucleate cells that surround the gland extension (Figure 1B). Formation of the gland projections has been suggested to occur by a process referred to either as the "fishing line model" or "retrograde extension" (Pilon 2008; Heiman and Shaham 2009). In this model, the glands attach to the pharyngeal lumen at the site of their birth and migrate posteriorly, forming their projections as a result of moving away from the anchor point of the duct. This model was first suggested by Sulston in his landmark article describing the *C. elegans* embryonic lineage (Sulston *et al.* 1983) and has since been demonstrated to occur in the formation of projections of several other *C. elegans* cells, including pharyngeal neurons, amphid neurons, and body wall muscles, as well as cells in higher organisms (including granule cells in the mammalian cerebellum) (Morck *et al.* 2003; Dixon and Roy 2005; Heiman and Shaham 2009). However, whether the pharyngeal glands use such a mechanism has not been established.

Postembryonically, the gland projections grow roughly twofold, in conjunction with growth of the pharynx. During this time, the glands retain their original points of connection to the lumen and maintain the morphology of the projections. Thus, another question is how the size and shape of the gland projections is regulated during growth of the entire animal. This problem is referred to as "scaling." In neurons, scaling can occur in response to tension along the axon as a result of organismal growth (Bray 1984) or by ongoing signaling between neurons and neighboring tissue during growth (Parrish *et al.* 2009).

To investigate morphogenesis of *C. elegans* glands and maintenance of their projections, we conducted a forward genetic screen to identify mutants with abnormal glands.

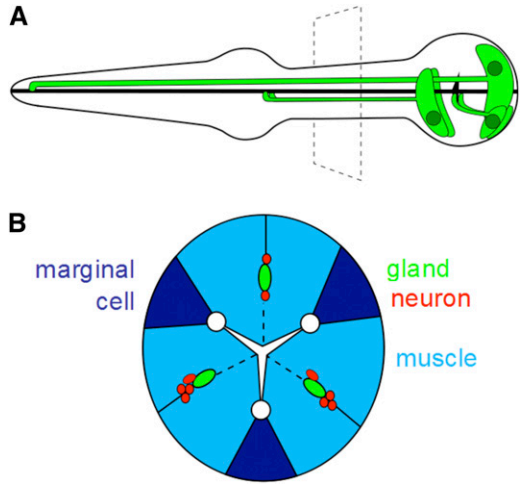

Figure 1 Anatomy of pharyngeal glands. (A) The pharynx of *C. elegans*, emphasizing the five glands (green cytoplasm, dark green nuclei). Anterior is at left, dorsal at top. At the top is the g1P gland, which has the longest gland projection, connecting to the pharyngeal lumen (thick black line) near the anterior end of the pharynx. The next longest projections belong to the two g1A glands (left and right, with the right gland largely hidden below the left in this diagram). Finally, the g2 glands (left and right) have the shortest projections, which connect near the pharyngeal grinder (black triangle). (B) Cross-section through the isthmus of the pharynx (as indicated by the dashed lines in A). Gland projections are bundled with the axons of pharyngeal neurons and surrounded by pharyngeal muscles. The surrounding musculature consists of two cells that have fused apically (dashed lines).

Our collection includes mutants in which the gland projections appear to be "overgrown," exhibiting swelling, branching, and apparent hypertrophy. This overgrowth generally worsens with age, suggesting inappropriate maintenance of gland size and structure during growth. Cloning of one such mutant revealed it to be an allele of the β-spectrin–encoding gene *sma-1*. Consistent with previous reports, we show that *sma-1* is expressed in the myoepithelial cells surrounding the glands, but not in the glands themselves, suggesting that the pharyngeal muscles play a role in maintenance of gland morphology. Accordingly, we find that several previously characterized mutants with defective or impaired pharyngeal muscles exhibit similar gland defects and we further provide evidence that the muscles normally maintain the shape of the gland projections. The results suggest a model in which maintenance of gland morphology and scaling of projections results from a balance of forces between ongoing gland growth and restraint by pharyngeal muscles.

Materials and Methods

Worm strains

Standard nematode handling conditions were used (Brenner 1974). All strains were grown at 20°, except where noted. Genes and alleles used were:

LG I: *unc-89(e1460)*, *let-502(sb118)*, *dpy-5(e61)*, and *let-381(gk302) I/hT2[bli-4(e937) let-?(q782) qIs48] (I;III)*.

LG II: *ivIs12 [phat-1*::*YFP elt-2*::*GFP rol-6(su1006)]* and *rol-6(e187) hlh-6(tm299) unc-4(e120)*.
LG III: *sma-2(e502)* and *sma-3(e491)*.
LG IV: *jcIs1[ajm-1*::*GFP rol-6(su1006)]*, *dpy-13(e184)*, and *let-60(sy101sy127)*.
LG V: *sma-1(e30)*.
LG X: *pha-2(ad472)*.

The integrated strain GD139 (*hlh-6*::*YFP*, *elt-2*::*LacZ*::*GFP*, *rol-6(su1006)*) was generated by gamma irradiation as described (Evans 2006) and was outcrossed to the wild-type N2 four times. Mutagenesis of GD139 was performed with ethylmethanesulfonate (EMS) as previously described (Brenner 1974). Individual L4 animals were picked from the mutagenized population to fresh plates and grown at 20°. Individual F_1 progeny were then picked and transferred to new plates and F_2 progeny screened under a fluorescent dissecting scope for gland defects. All of the mutants isolated in this screen are homozygous viable. Single nucleotide polymorphism (SNP) mapping was performed by bulk segregant analysis (BSA), as described (Davis *et al.* 2005).

For most tests of gland morphology, we either crossed *ivIs12* into the mutant background to label glands or generated new extrachromosomal transgenes by injecting the *phat-1*::*YFP* reporter into the desired mutant background (indicated as "Ex" in Table 1). We examined either L1 animals or adults (collected ~96–108 hr after egg laying). To score gland "defects," we counted any animal in which the gland projections exhibited any blebbing, swelling, or branching. Some of these defects may be normal variations in gland morphology. For example, in older wild-type adults we observe infrequent (<5%) and minor varicosities that may be associated with age-related decline (Garigan *et al.* 2002). However, these effects are relatively small, allowing us to readily detect alterations in gland morphology associated with a number of different genetic backgrounds. We have generated numerous transgenic lines with the *phat-1* reporter in wild-type animals and have not observed significant gland defects associated with the presence of this (or other) transgenes. Additionally, extrachromosomal transgenes always faithfully recapitulate the expression pattern seen in *ivIs12*.

In the course of mapping one of the mutants obtained in the screen (allele *iv52*), we discovered that the original strain carrying the integrated transgenes (GD139) has a probable inversion on the right arm of LG II. SNP mapping of *iv52* (and of *iv36*) revealed a lack of recombination between N2 and CB4856 (Hawaiian) chromosomes along the right arm of LG II from +4 to +22, suggestive of a chromosomal rearrangement. We therefore examined the original (unmutagenized) strain, GD139, and discovered the same repression of recombination on LG II, suggesting that the rearrangement exists in the parent strain (Supporting Information, Figure S1). This rearrangement likely resulted from the integration of the *phat-1*::*YFP* transgene, which maps to the same region of the genome. The rearrangement is most likely an inversion (rather than a transposition), as no other region of the genome showed suppression of recombination (data not shown). Importantly, the parent strain has normal glands and appears healthy, indicating that the rearrangement did not result in a gland phenotype. However, during our subsequent analysis of mutants, we were conscious of the possibility that the rearrangement might have a subtle influence on mutant phenotypes (*e.g.*, might act as a modifier), and where possible, gland phenotypes were examined using a second, unintegrated reporter. Because the integration event appears to substantially suppress recombination along the right arm of LG II, this strain may be useful as a balancer for this region of the genome.

Table 1 Gland projection defects in different mutants

Strain	Stage	Transgene	Gland projections: WT (%)	Gland projections: Abnormal (%)	*N*
+/+; *ivIs12*	L1	*ivIs12*	100	0	57
sma-1(iv38)	L1	*ivIs12*	13	87	132[b]
let-502(sb118ts) @ 15°	L1	Ex	98	2	40
let-502(sb118ts) @ 25°	L1	Ex	8	92	36[b]
pyr-1(RNAi inj)	L1	*ivIs12*	38	62	39[b]
unc-52(RNAi inj)	L1	*ivIs12*	25	75	48[b]
tnt-4(RNAi inj)	L1	*ivIs12*	0	100	37[b]
let-381(gk302)	L1	Ex	100	0	39
let-60(sy101sy127)	L1	Ex	100	0	42
ztf-11(ok646)	L1	Ex	100	0	40
elt-2(RNAi feed)	L1	*ivIs12*	100	0	79
+/+; *ivIs12*	Adult	*ivIs12*	96	4[a]	50
+/+; *ivEx*	Adult	Ex	98	2[a]	50
iv37	Adult	*ivIs12*	43	57	61[b]
iv50	Adult	*ivIs12*	23	71	66[b]
sma-1(iv38)	Adult	*ivIs12*	0	100	86[b]
sma-1(e30)	Adult	*ivIs12*	1	99	77[b]
unc-89(e1460)	Adult	Ex	53	47	109[b]
tnt-4(RNAi -inj 1/2)	Adult	*ivIs12*	37	63	51[b]
pha-2(ad472)	Adult	Ex	0	100	52[b]
sma-2(e502)	Adult	*ivIs12*	93	7[a]	81
sma-3(e491)	Adult	*ivIs12*	89	11[a]	71
dpy-5(e61)	Adult	*ivIs12*	95	5[a]	42
dpy-13(e184)	Adult	*ivIs12*	94	6[a]	72
tnt-3(RNAi inj)	Adult	*ivIs12*	94	6[a]	128

To visualize glands, animals carried either an integrated *phat-1*::*YFP* transgene (*ivIs12*) or an extrachromosomal array (Ex) generated by microinjection of DNA into the mutant strain. Use of different transgenic arrays (extrachromosomal *vs.* integrated) did not appear to have any influence on gland morphology. The *ztf-11 (ok646)* strain produces 16% L1 lethals; all of the animals scored here were L1 lethal. RNAi was performed either by injection (inj) or by feeding (feed); see *Materials and Methods* for details.

[a] Apparent background levels of gland "abnormalities," possibly representing normal variation in gland morphology or a minor effect caused by transgenes. We typically observe infrequent and minor defects in older adults that may result from age-related decline of animals.

[b] The frequency of defects was significantly greater ($P < 0.001$, χ^2 goodness-of-fit, 2 d.f.) compared to wild type. In all other cases, the frequency of defects was not significantly different than wild type ($P > 0.3$, χ^2 goodness-of-fit, 2 d.f.).

Construction of plasmids

GFP reporters (*ceh-2*::*GFP*, *dlg-1*::*GFP*, and *sma-1*::*GFP*) were made by PCR amplification from genomic DNA followed by cloning of fragments into the GFP expression vector pPD95.77. Oligonucleotides used to amplify genomic

fragments are listed below; lowercase sequence indicates engineered ends to facilitate cloning.

ceh-2: aactgcagAAGTGCGGACAATGATTCTAGGTTC and cgg ggtaccTTCACTCCGAATATTAGAAAAAATAAGTAAACTAG; cloned as *Pst*I/*Kpn*I fragment; the resultant reporter contains ~1.2 kb of sequence upstream of the predicted ATG of *ceh-2*, comparable to other published *ceh-2* reporters (Aspock *et al.* 2003).

sma-1: aactgcagATTCGTGGCGTCCCGGAGAGT and cggggta ccGATACCCTTCTACCTTGTCTGAAAAATATACATT; cloned as *Pst*I/*Kpn*I fragment; the resultant reporter extends to the second exon of the *sma-1a* isoform and is diagrammed in Figure 3. The *sma-1*::*GFP*::*His2B* construct was made by replacing the GFP cassette of the *sma-1*::*GFP* reporter with the *GFP*::*His2B* cassette from plasmid pAP.10 (Gaudet and Mango 2002).

dlg-1: GGCGCGTTTGAAAATGAGGACCGAGTG and ctggtac cACATTTTCTATCGCTTTATGCGCTTCTG; cloned as AgeI/*Kpn*I fragment; the resultant reporter contains ~3 kb of upstream sequence as well as the first exon and intron of the *dlg-1a* isoform.

Additional details of plasmids and cloning strategies are available upon request.

Construction of transgenic lines

Transgenes were injected at 10–20 ng/μl together with 50 ng/μl pRF4 [*rol-6(su1006)*] (Kramer *et al.* 1990; Mello *et al.* 1991) and pBSII SK$^+$ to a total DNA concentration of 100 ng/μl.

RNAi

RNAi was performed by injection of dsRNA prepared from Ahringer library clones, as previously described (Fire *et al.* 1998; Kamath *et al.* 2003). dsRNA was injected at 1 μg/μl, except where noted. In the case of *elt-2*, we performed RNAi by feeding, as previously described (Timmons and Fire 1998), as *elt-2(RNAi)* gives a highly penetrant (~100%) L1 lethality by feeding (McGhee *et al.* 2009).

Volume measurements

To estimate gland cell volumes, images from adult transgenic animals were collected as a *Z* series at 0.8-μm intervals using a Zeiss AxioCam and ApoTome, supported by Axiovision 4.8 software. For each optical section, we measured the area of the GFP$^+$ regions using ImageJ (Rasband 1997–2010). Area measurements were then summed for each structure to provide an estimate of GFP$^+$ volumes.

Transmission electron microscopy

For electron microscopy, worms were anesthetized in 5 mM levamisole and were decapitated with a 27 gauge × 1/2 Monoject needle. Heads were fixed in 3% glutaraldehyde in Millonig's phosphate buffer for 1 hr at room temperature. Postfixation was in 2% OsO_4 for 20 min. Samples were dehydrated in ethanol and infiltrated with Polybed 812 resin (Polysciences). Polymerization was performed at 60° for 48 hr. Silver-gray sections were cut with an ultramicrotome (Leica) equipped with a diamond knife, and sections were stained with uranyl acetate and lead citrate and examined in a H-700 Hitachi electron microscope.

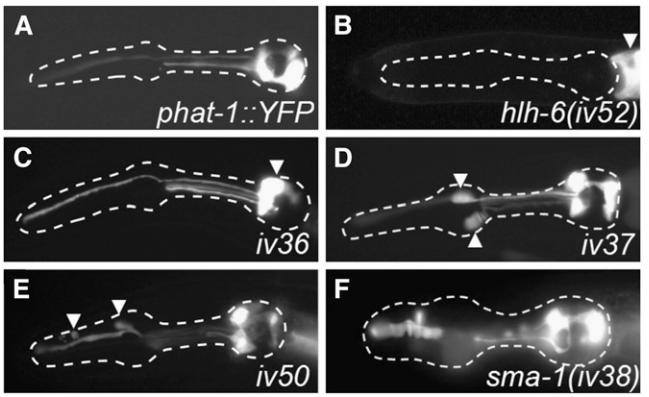

Figure 2 Representative images of wild-type parent strain (GD139) and mutants with gland defects. In all images, the open dashed line indicates the outline of pharynx, and anterior is at left. (A) GD139 *ivIs12 [phat-1*::*YFP elt-2*::*GFP]* larvae. (B) Expression of the *phat-1* reporter is lost in *hlh-6 (iv52)* animals but *elt-2*::*GFP* expression (to mark the presence of the transgene) in the intestine is unaffected (arrowhead). (C) Cell body of g1P gland (arrowhead) is found anterior of its normal position and g2 glands are not visible in *iv36* homozygotes. (D) *iv37* mutants show abnormal swelling of gland projections in the anterior pharyngeal bulb (arrowheads). (E) Abnormal swelling of gland projections in the anterior pharynx of *iv50* homozygote (arrowheads). (F) *sma-1(iv38)* mutants exhibit severe swelling and occasional branching of gland projections, and the pharynx is incompletely elongated.

Laser microsurgery

L2-adult stage hermaphrodites were mounted in 1 μl of 10 mM muscimol (Sigma M1523) in M9 on a 5% agarose pad under a coverslip. GFP expressing g1P gland cells were imaged with a Microradiance 2000 confocal microscope using a Nikon 60X, 1.4 NA lens. Gland cell processes were cut using a 440-nm MicroPoint Laser System from Photonic Instruments. After surgery, animals were recovered to an agar plate seeded with HB101, and remounted for confocal imaging 1–3 days postsurgery. Regeneration was scored in nine animals in which successful cuts were made at the L2 stage.

Results

Genetic screening identifies a variety of gland defects

Gland projections are proposed to develop during embryogenesis, as gland cells migrate from their site of birth to their final position in the pharynx (Sulston *et al.* 1983). Glands may therefore form attachments to the pharyngeal lumen at the site of their birth, with the gland projection being drawn out as the gland cell migrates posteriorly. To investigate development of pharyngeal glands and their extensions, we

performed a genetic screen for animals with gland defects. We screened animals carrying an integrated, gland-specific YFP reporter (*phat-1*::*YFP*) for any alterations to gland cell number or morphology. A screen of ~5000 haploid genomes identified five recessive mutants (Figure 2). Of these five mutants, one (*iv52*) lacked observable gland reporter expression, one (*iv36*) lacked expression in a subset of glands and showed apparent defects in g1P migration, and three (*iv37*, *iv38*, and *iv50*) had wild-type numbers of expressing cells with abnormal morphology of the gland extensions.

Isolation of a new allele of hlh-6

By genetic mapping, complementation, and allele sequencing, we find that the mutant lacking observable reporter expression (Figure 2B), *iv52*, is an allele of the previously characterized gene *hlh-6*, which encodes a bHLH transcription factor that is required for expression of many gland genes, including *phat-1* (Raharjo and Gaudet 2007; Smit *et al.* 2008). Homozygous *iv52* animals have the same phenotype as *hlh-6(tm299)* homozygotes, which carry a deletion allele predicted to be a molecular null (Smit *et al.* 2008), and *iv52* fails to complement *hlh-6(tm299)*. Sequencing of *hlh-6* from *iv52* homozygotes identified a single nucleotide change in the coding region, 544G > A (position is relative to the start of the cDNA), which results in a Glu-to-Lys (E182K) missense mutation in the predicted product (Figure S2). This mutation lies in the predicted DNA binding domain of HLH-6 and affects a glutamate residue that, in other bHLH proteins, makes direct contact with the E-box, the DNA binding site for bHLH proteins (Ma *et al.* 1994). Molecularly, this alteration is predicted to be a strong loss of function, which is consistent with our observation that *iv52* animals are phenotypically indistinguishable from *tm299* animals.

Isolation of mutant affecting gland cell body position

Another mutant, *iv36*, lacks observable expression of *phat-1*::*YFP* only in the g2 glands, while all three g1 glands are visible. Interestingly, the g1P cell body occupies a position anterior to its wild-type location, yet the gland projections of all three g1 cells appeared normal (Figure 2C). This phenotype supports the retrograde extension model for formation of the g1P gland extension in that the mutant appears to be defective for migration of g1P. However, there may be other explanations for this phenotype that we are currently investigating. This mutant mapped to the right arm of chromosome II, but further mapping was prevented by the probable inversion in this region that likely resulted from the integration of the *phat-1*::*YFP* transgene (see *Materials and Methods*). Whole-genome sequencing or isolation of other alleles (using a different transgenic strain lacking the inversion on II) will allow identification of the relevant gene.

Mutants affecting morphology of the gland projection

The remaining three mutants, *iv37*, *iv38*, and *iv50*, all affect gland morphology to varying degrees (Figure 2, D–F). SNP mapping placed these mutants at three different map positions, indicating that each mutation affects a different gene. Two of these mutations (*iv37* and *iv50*) result in variable defects in the gland extensions. In *iv37* homozygotes, defects are restricted to the anterior bulb region of the pharynx, with 57% (n = 61) of animals showing defects in the g1P and/or the g1A cells. Initial BSA–SNP mapping placed *iv37* on the right arm of LG III. In *iv50* mutants, defects are not restricted to the anterior bulb region, but are instead visible along the anterior half of the pharynx in 71% (n = 66) of animals. BSA–SNP mapping placed *iv50* in the middle of LG III.

The final mutation, *iv38*, resulted in striking gland defects in 100% of examined animals. Animals homozygous for *iv38* have normal gland cell bodies and all glands appear to connect with the pharyngeal lumen at their normal positions. However, the gland projections have a variety of abnormalities, including additional branching, swelling, and thickening, and abnormal trajectories (Figure S3). The gland defects are not the result of general defects in pharyngeal cellular morphology, as the pharyngeal neuron I3 (which lies in direct contact with the anterior portion of the g1P projection) appears normal in *iv38* animals. We examined *iv38* animals with a *ceh-2*::*GFP* marker that is expressed in I3 (and other neurons) (Aspock *et al.* 2003). Of 35 *iv38*; *ceh-2*::*GFP* animals examined, 89% had normal-looking I3 neurons, while 11% showed minor "blebs" along the axon. We scored *iv38* animals with a different, unintegrated reporter (*hlh-6*::*mTomato*). These animals also showed 100% penetrance of gland defects (data not shown), arguing that the phenotype is specific to *iv38* and is not caused or enhanced by the inversion associated with *ivIs12*. Given the severity and 100% penetrance of the gland phenotype in these mutants, we chose to examine *iv38* in more detail.

iv38 is an allele of sma-1

In addition to their gland defects, *iv38* homozygotes are smaller (Sma) than wild-type animals of the same developmental stage and are somewhat dumpy (Dpy) in appearance. However, mutations in other *dpy* genes (that result in smaller body size; *dpy-5* and *dpy-13*; Table 1) have no effect on gland morphology, suggesting that the gland defects are not simply a byproduct of defects in body size. SNP mapping placed *iv38* in a region on LG V between +0.5 and +5.6. We searched this region for genes associated with a Dpy or Sma phenotype, either by mutation or RNAi, and identified *sma-1* as a candidate gene. We determined that *iv38* is an allele of *sma-1* by three criteria. First, we examined pharyngeal glands in *sma-1(e30)* mutants and found that these animals exhibited the same defects observed in *iv38* homozygotes (Figure 3, D and E). Second, we found that *e30* and *iv38* failed to complement each other with respect to both the gland phenotype and the Sma phenotype. Third, we sequenced *sma-1* in *iv38* homozygotes and found a single mutation at position 5253 of the cDNA (5253G > A), which changes a Trp codon to a stop codon (W1751Stop; Figure 3B).

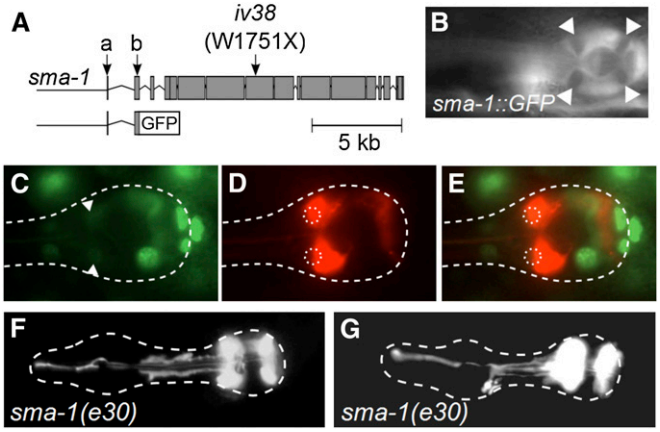

Figure 3 (A) Schematic of *sma-1* gene, indicating the newly isolated nonsense mutation, *iv38*, and the structure of the *sma-1*::*GFP* reporter; a and b designations indicate start positions of each of two *sma-1* isoforms. (B) Expression of *sma-1*::*GFP* in the posterior pharyngeal bulb. Expression is visible in the myoepithelial cells but is absent from pharyngeal glands (arrowheads). (C–E) Nuclear *sma-1*::*GFP*::*HIS2B* is absent from gland cells; dorsal view of posterior pharyngeal bulb (outlined). (C) *sma-1*::*GFP*::*HIS2B* is evident in nuclei of pharyngeal muscles and marginal cells; arrowheads indicate weak GFP signal from out-of-plane pm5 pharyngeal muscle nuclei. (D) *phat-1*::*wCherry* in g1A glands, with dotted circles showing position of pm5 nuclear signal; no nuclear GFP is evident within the gland cells. (E) Merge of images from C and D, with pm5 nuclei outlined. (F and G) Gland morphology in *sma-1(e30)* mutants resembles that seen in *sma-1(iv38)* mutants.

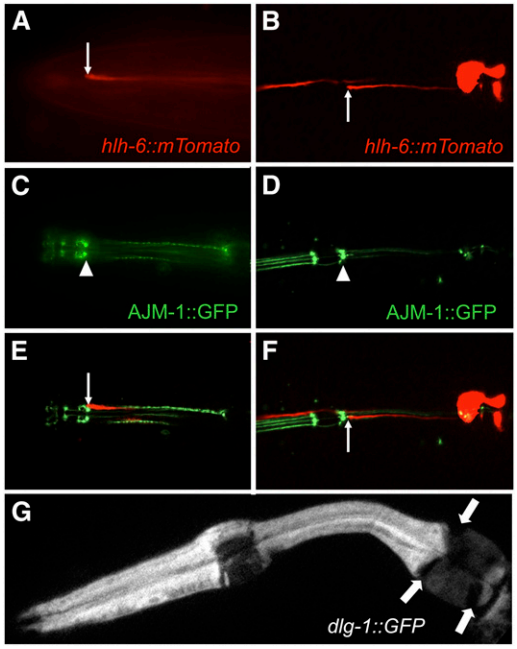

Figure 4 Glands lack expression of epithelial markers. (A and B) Expression of *hlh-6*::*mTomato* in pharyngeal glands. Arrows indicate the anterior ends/ducts of g1P (A) and one of the g1A cells (B). (C and D) Expression of a rescuing AJM-1::GFP translational fusion in the same regions as A and B; arrowheads indicate the location of the gland ducts. (E and F) Merge of *hlh-6*::*mTomato* and AJM-1::GFP expression; there is no apparent overlap of expression in the gland ducts. (G) Expression of a *dlg-1*::*GFP* reporter shows a lack of expression in the pharyngeal glands (arrows).

The *sma-1* gene encodes a β_H-spectrin that is expressed in *C. elegans* epithelial cells and is a component of the membrane cytoskeleton (McKeown *et al.* 1998; Norman and Moerman 2002; Praitis *et al.* 2005). Mutations affecting *sma-1* result in a smaller body size due to defects in embryonic elongation, consistent with its expression in epithelial cells. SMA-1/β_H-spectrin forms part of the apical membrane cytoskeleton and is thought to play a role in stabilizing interactions between this network and the actin cytoskeleton during morphogenesis. Gland defects in *sma-1* mutants could result either from structural defects in the gland themselves or from defects in the surrounding pharyngeal muscles. Previous reports, using both reporter transgenes and α–SMA-1 immunostaining, do not indicate SMA-1 expression in glands, a finding that we verified using a *sma-1* transcriptional reporter, which includes the entire upstream intergenic region and first intron of the *sma-1a* isoform (which would include any and all upstream sequence of the *sma-1b* isoform). We observed expression of *sma-1*::*GFP* in all epithelial cells, as expected (hypodermis, excretory canal cell, intestine, pharyngeal muscles, and pharyngeal marginal cells) (McKeown *et al.* 1998) but saw no observable expression in gland cells (Figure 3C). Likewise, use of a nuclear-localized *sma-1*::*GFP*::*HIS2B* reporter did not indicate any expression in gland nuclei (Figure 3D).

This finding raised the possibility that gland defects in *sma-1* animals are a consequence of defects in the surrounding musculature and further suggests that glands lack epithelial characteristics. Accordingly, glands also lack expression of components of the adherens junctions, which are markers of epithelial identity. Previous reports suggested that the gland duct, which connects the gland projection to the pharyngeal lumen, contains adherens junctions (Albertson and Thomson 1976). However, our results suggest that the glands do not express at least two of the components of the adherens junctions, AJM-1 and DLG-1(Mohler *et al.* 1998; McMahon *et al.* 2001). Neither a rescuing AJM-1::GFP translational fusion nor a *dlg-1* transcriptional reporter are visible in gland cells (Figure 4), suggesting that while the duct may be associated with adherens junctions, the glands themselves must express some other molecule(s) that facilitate connection to the pharyngeal lumen.

Since glands appear to lack *sma-1* expression, one possible explanation for the *sma-1* gland phenotype is that pharyngeal muscles normally function to constrain growth of the glands and that, in *sma-1* mutants, the defective muscles are unable to adequately restrain gland growth. Consistent with a model in which muscles constrain growth of the glands, we observed that the gland phenotype becomes progressively more severe as animals develop. In newly hatched *sma-1* larvae (L1s), 67% had relatively mild defects in gland morphology and 20% had moderate-to-severe defects (the remaining 13% appeared normal; $n = 132$). In contrast, 100% of young *sma-1* adults exhibited moderate-to-severe defects ($n = 86$) (Table 1). One possibility is that, as

Table 2 Mean pharynx length in adult animals (±SD)

Strain	Pharynx length (μm)	*N*
N2	140 ± 3	37
sma-1(iv38)	97 ± 4	10
sma-2(e502)	110 ± 4	10
sma-3(e491)	106 ± 2	38

In all three *sma* mutants, mean pharynx length is significantly smaller than that of N2 ($P < 0.001$, Student's *t*-test).

animals grow, growth of glands is counterbalanced by forces exerted by the surrounding musculature. If this force is weakened, as in *sma-1* mutants, then growth of glands during development would be relatively less constrained, resulting in the types of overgrowth defects seen here.

An alternate possibility, which cannot be ruled out from these studies, is that SMA-1 is present and functional in pharyngeal glands, but not detected by our reporter or by previous analyses. An ideal approach would be to test rescue of the gland phenotype by expressing *sma-1* under the control of tissue-specific promoters (*e.g.*, gland-specific or muscle-specific promoters). Unfortunately, the large size of the *sma-1* gene (>12 kb cDNA) proved challenging with respect to the cloning of such rescuing constructs. Therefore, to test the hypothesis that pharyngeal muscle integrity influences gland morphology, we chose to examine several other mutants with impaired pharyngeal muscle structure and/or function.

Defects in pharyngeal muscles result in abnormal gland morphology

To test the general hypothesis that the pharyngeal muscles are important in maintenance of gland morphology, we examined glands in two classes of mutants: those in which pharynx size was reduced but in which pharyngeal muscles were otherwise normal and those in which pharyngeal elongation and/or muscle structure were impaired. In the experiments that follow, we scored either young adults (if mutants were viable) or arrested embryos and/or L1 larva (if mutants were lethal).

One possible explanation for the gland defects in *sma-1* mutants is that the glands are growing to normal size/volume while contained in a smaller pharynx. We therefore examined other mutants with reduced pharynx size, namely *sma-2* and *sma-3*, which encode downstream signaling components of a TGFβ signaling pathway required for normal *C. elegans* size (Savage *et al.* 1996). Unlike *sma-1* mutants, *sma-2* and *sma-3* mutants undergo normal elongation and have normal pharyngeal morphology, but are smaller than wild type due to reduced postembryonic growth of cells. Although not previously reported, we find that the average pharynx length in *sma-2* and *sma-3* adult animals is significantly smaller than that of wild-type animals of the same age (Table 2). However, the glands of *sma-2* and *sma-3* mutants do not show any apparent defects (Figure 5A, Table 1). Thus, one interpretation is that the gland defect in *sma-1* mutants is not due to the smaller pharynx size, but rather

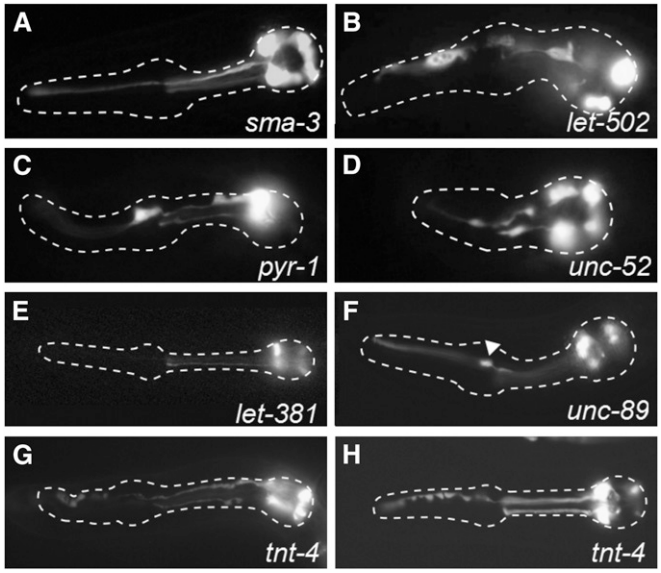

Figure 5 Gland defects associated with different pharyngeal muscle mutants. All images are of *phat-1*::*YFP* expression and the dashed line outlines the pharynx. (A) *sma-3(e491)*; *phat-1*::*YFP* adult. (B) *let-502 (sb118ts)*; *phat-1*::*YFP* L1 larvae grown at 25°. (C) *pyr-1(RNAi)*; *phat-1*::*YFP*, L1 larvae. (D) *unc-52(RNAi)*; *phat-1*::*YFP*, arrested embryo. (E) *let-381*; *phat-1*::*YFP*. (F) *unc-89(e1460)*; *phat-1*::*YFP*; arrowhead indicates protrusion from anterior end of g1A projection. (G) *tnt-4(RNAi)*; *phat-1*::*YFP*, arrested L1 from 1 mg/ml dsRNA injection. (H) *tnt-4(RNAi)*; *phat-1*::*YFP* adult from 0.5 mg/ml dsRNA injection.

due to defects in elongation and/or structure of the pharyngeal muscles. An alternate interpretation is that glands are normal in *sma-2* and *sma-3* mutants because all cells (including glands) are smaller in these mutants. However, on the basis of our analyses of glands in other mutants (below), we propose that glands in *sma-1* mutants are defective because of defects in pharyngeal muscle integrity rather than the smaller size of the pharynx.

One aspect of the *sma-1* mutant phenotype is incomplete elongation of both the embryo and the pharynx. Embryonic elongation occurs as a result of contractions of the actin cytoskeleton of the lateral epidermal cells (seam cells) (Priess and Hirsh 1986; Chisholm and Hardin 2005; Gally *et al.* 2009). These contractions are regulated by a network of genes including the Rho kinase encoded by *let-502*. Depletion of maternal and zygotic *let-502* results in arrest after hatching as unelongated larvae (Wissmann *et al.* 1997). Using the temperature-sensitive mutation *let-502(sb118)* (P. Mains, personal communication), we found that glands in *let-502* mutants raised at the restrictive temperature (25°) showed the same types of defects present in *sma-1* hatchlings (Figure 5B, Table 1), while glands in animals raised at the permissive temperature (15°) were normal, suggesting that defects in elongation lead to defects in gland morphology.

Loss of function of other genes required for elongation resulted in consistent gland defects resembling those seen in *sma-1* mutants. RNA-mediated interference (RNAi) of *pyr-1*,

which encodes a CAD protein with three enzymatic activities (Carbamoyl phosphate synthetase, Aspartate transcarbamoylase, and Dihydroorotase) that is involved in pyrimidine synthesis (Franks *et al.* 2006), causes an incompletely penetrant early arrest, in which animals have unelongated or incompletely elongated pharynges (as well as other morphological defects). *pyr-1(RNAi)* animals display gland defects that correlate with the severity of the pharyngeal phenotype. For example, viable *pyr-1(RNAi)* progeny have apparently normal glands while arrested larvae with pharyngeal defects have abnormal glands (Figure 5C). A similar result was obtained by RNAi against *unc-52*, which encodes the basement membrane component perlecan; disruption of *unc-52* results in embryonic arrest midway through elongation (paralyzed arrest at twofold, Pat, phenotype) (Rogalski *et al.* 1993). *unc-52(RNAi)* resulted in 100% embryonic arrest, accompanied by frequent gland defects similar to those seen in *sma-1* embryos and L1 larvae. We conclude that the gland defects in the above mutants specifically result from defects in elongation rather than being merely a consequence of embryonic or larval arrest, as other lethal mutations that we have tested do not result in defects in gland projections (*let-381*, *let-60*, *ztf-11*, and *elt-2*; Figure 5D, Table 1) (Han and Sternberg 1990; Maeda *et al.* 2001; McGhee *et al.* 2009; Amin *et al.* 2010).

We also examined mutants in which pharyngeal elongation was normal but where muscle structure was impaired. We examined the effects of mutation in *unc-89*, which encodes an M-line–specific component of the actin-myosin contractile apparatus (Benian *et al.* 1996), and RNAi-mediated knockdown of two pharyngeal troponin T genes, *tnt-3* and *tnt-4*. These mutants are expected to affect integrity of the musculature but not elongation of the pharynx, in contrast to *sma-1* mutants. Importantly, the genes being tested are known to be expressed and act specifically in muscles (either pharyngeal muscle only or in both pharyngeal and nonpharyngeal muscles) and not in pharyngeal glands. The *unc-89 (e1460)* mutation is a hypomorphic allele in which UNC-89 product is produced but leads to defects in muscle fiber organization with little or no M-line (Waterston *et al.* 1980; Benian *et al.* 1996); this allele, unlike the null, is viable and moves normally. Mutants have normal pharynx morphology, but gland projections are frequently defective, with 47% of mutants exhibiting swelling of projections or outgrowths along their length (Figure 5F). While this phenotype is less severe than that of *sma-1*, it is likely to reflect the hypomorphic nature of the *unc-89(e1460)* allele.

Removal of a pharynx muscle-specific troponin T (*tnt-4*) results in gland defects like those seen in *sma-1* (and other) mutants. *C. elegans* contains four predicted troponin T genes, *tnt-1–4*, two of which (*tnt-3* and *tnt-4)* are expressed in pharyngeal muscles (Kohara 2001a,b; Amin *et al.* 2007). RNAi against *tnt-3* had little effect (Table 1). In contrast, RNAi against *tnt-4* resulted in L1 arrest, presumably due to a reduction in pharyngeal pumping and subsequent starvation. Overall pharyngeal morphology of *tnt-4(RNAi)* animals was unaffected, suggesting that TNT-4 is not required for pharyngeal elongation, but rather for pharyngeal function. However, gland morphology was abnormal in all *tnt-4 (RNAi)* animals, consistent with a role for muscle in constraining growth of gland extensions (Figure 5G). We also tested a sublethal dose of *tnt-4* dsRNA. The resulting adults had normal pharyngeal morphology and size but showed frequent defects in gland morphology (Figure 5H, Table 1).

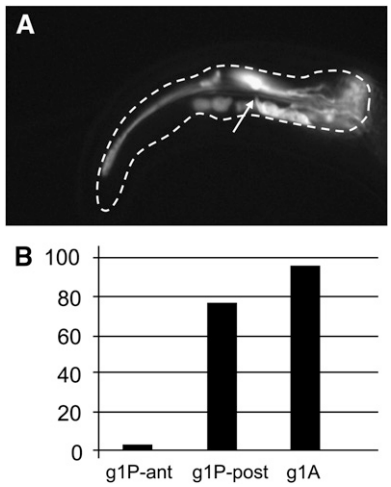

Figure 6 Gland defects in *pha-2(ad472)* mutants. (A) Gland projections in the posterior pharynx are severely misshapen in *pha-2* mutants. Arrow indicates the normal position of the g1A duct, which appears to still be present. Note that the longest projection, from g1A, has defects in the posterior (right) half of the pharynx while the anterior portion of the projection looks normal. (B) Gland defects in *pha-2* mutants are largely restricted to the posterior pharynx; shown is percentage of mutants with moderate-to-severe defects in the anterior or posterior halves of the g1P projection (g1P-ant and g1P-post, respectively) and for the g1A gland projections, which reside in the posterior half of the pharynx ($n = 52$).

Finally, we examined a mutant (*pha-2*) in which only a subset of pharyngeal muscles is defective. In *pha-2* mutants, the pharynx is incompletely elongated, exhibiting a shortened pharyngeal isthmus as a result of defects in the differentiation of the pm5 muscles (Avery 1993; Morck *et al.* 2004). Accordingly, *pha-2* is expressed in a subset of pharyngeal muscle cells, including pm4 and pm5, but is absent from the pharyngeal glands (Morck *et al.* 2004, 2006). In *pha-2* mutants, the gland projections display severe abnormalities like those seen in *sma-1* mutants (Figure 6A). As with *sma-1*, the gland phenotype becomes more severe as *pha-2* animals develop, with late larvae and adults having grossly swollen gland projections. Interestingly, the defects in the gland projections are largely confined to the posterior pharynx (Figure 6B). The anterior portion of the longest projection (from g1P) is normal; this projection is surrounded by the pm2 and pm3 muscles, which are unaffected in *pha-2* mutants. Dramatically, the posterior portion of the g1P projection and the whole of the g1A projections are defective. These projections are surrounded by the pm4 and pm5 muscles, where *pha-2* functions. The localized nature of the gland defects in *pha-2* mutants, corresponding to

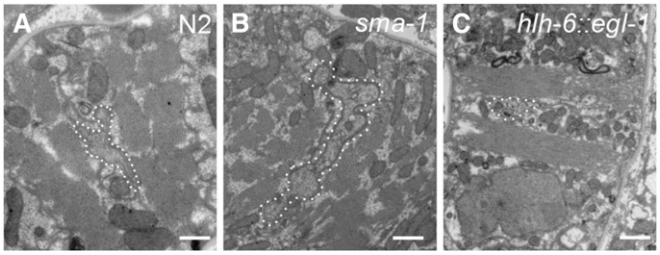

Figure 7 Transmission electron microscopic analysis of gland projections in pharyngeal cross-sections. In all images, sections are through the pharyngeal isthmus (between the two pharyngeal bulbs) of adults. Bar in each image, 500 nm. (A) Wild type, with projection of g1P gland outlined by open dots. (B) *sma-1(iv38)*, with abnormally large g1P projection outlined. (C) *hlh-6*::*egl-1* animal, with subventral pharyngeal nerve cord outlined (containing the axons of M2, M4, I4, and I5; the NSM axon is separate from the nerve cord, to the right of the image); the g1A gland projection is normally present in this structure, but is absent due to the induction of apoptosis in glands by *hlh-6*::*egl-1*.

the region where *pha-2* results in muscle defects, strongly supports the hypothesis that the gland projection defects result from defects in the immediately surrounding musculature.

Analysis of gland projections by transmission electron microscopy

Taken together, the results from the various mutants argue that the morphology of the gland projections is influenced by the integrity of the surrounding pharyngeal musculature. The implication of this model is that the muscles and glands exert balancing pressure on one another, with a decrease in the pressure exerted by muscles resulting in apparent overgrowth of the glands. To consider this possibility in more detail, we examined pharyngeal cross-sections by transmission electron microscopy (TEM) of wild-type and *sma-1 (iv38)* animals. Consistent with the observations with the *phat-1*::*YFP* reporter, the gland projection in *sma-1* animals is considerably overgrown compared with wild type (Figure 7, A and B). We also note that although the *sma-1* gland is considerably larger, in both mutant and wild type there are no significant gaps or spaces between cells. This observation is consistent with a model in which gland growth is normally physically constrained by the surrounding musculature. When the muscles are impaired or defective, gland projections exert sufficient force to expand within the space between adjacent muscles. As a corollary to this model, we predict that a decrease in the force of gland growth would result in greater musculature inhibition of gland projections.

An alternative explanation for the overgrowth of the glands is that defects in pharyngeal muscle structure results in hollow spaces between adjacent cells, and that the glands simply grow to occupy preexisting intercellular gaps. To test this possibility, we examined the structure of pharyngeal muscles when the glands had been removed, to determine whether any such spaces would occur between glands. Gland-specific apoptosis can be induced by expressing the proapoptotic gene *egl-1* under the control of the *hlh-6* promoter (*hlh-6*::*egl-1*) (Smit *et al.* 2008). TEM of *hlh-6*::*egl-1* revealed that, in the absence of glands or gland projections, the pharyngeal muscles enclose any space where the glands would have been, *i.e.*, there are no intercellular gaps into which the glands might grow. Thus, the overgrowth of glands is more likely to occur because of an imbalance in forces exerted by the glands and muscles, with the glands and muscles effectively "pushing" against one another.

Increased volume of gland projections in sma-1 mutants

The gland projections in *sma-1* (and other) mutants appear to be larger than those of wild-type animals, both by live imaging with a cytoplasmic GFP and in TEM cross-sections. To estimate the volume of the gland cell bodies and of the g1P projection, we measured GFP^+ areas in optical sections from wild type and *sma-1* mutants. For these measurements, we examined the subset of *sma-1* mutants with relatively severe g1P defects, as assessed using a fluorescence dissecting microscope. Because of significant overlap of gland cell bodies, we cannot reliably distinguish the boundaries of the cells and instead measured total cell body volume (*i.e.*, total volume of all five gland bodies). Nonetheless, the average volume of the cell bodies (in arbitrary units) is not significantly different between *sma-1* mutants and wild-type animals (44,060 $\pm$ 7730 and 40,190 $\pm$ 1170, respectively; $n = 3$ of each genotype, $P > 0.05$, Student's *t*-test). In contrast, the estimated volume of the g1P projection was ~1.5-fold larger in *sma-1* mutants than in wild type (10,690 $\pm$ 200 and 7120 $\pm$ 710, respectively; $n = 3$ of each genotype, $P < 0.005$, Student's *t*-test), even though the length of the projection is ~70% that of wild type. The estimated volume measurement is consistent with measurements of EM photomicrographs, in which the cross-sectional area of the g1P projection is ~2.5-fold larger in *sma-1* compared to WT (Figure 7 and data not shown). Thus it is not the case that the increase of gland cell projection volume resulted in a redistribution of cytoplasm or a uniform increase in gland cell volume. These results suggest that in wild-type animals, the pharyngeal muscles not only shape the gland projection but also restrict its growth.

Gland projections exhibit limited growth following laser severing

If glands are normally constrained by pharyngeal muscles, then a decrease in the pressure exerted by the glands (or an increase in the pressure exerted by the muscles) would be expected to prevent their growth. To test this prediction, we performed laser microsurgery on gland projections in larvae in which the gland projections were fully formed and examined the gland projections in subsequent development. Normally, glands continue to grow throughout the life of the animal, keeping pace with growth of the pharynx and the rest of the body. We imagined three possible outcomes following laser severing, depending on the capacity of the gland to grow and the relationship between the glands and the

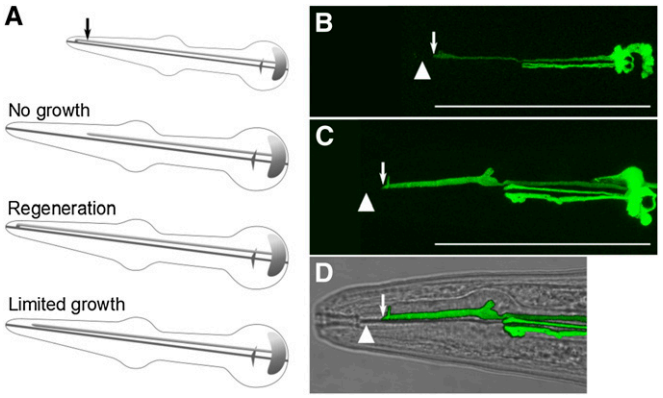

Figure 8 Gland projections continue to grow following laser severing. The longest gland projection (that of g1P) was laser severed in L2 animals and examined in adult animals. (A) Possible outcomes are no growth of the gland projection, regeneration of the projection, or limited growth. See text for more explanation. (B) Laser severing was performed in L2 animals, within ~5 μm of the g1P duct; arrow indicates point of severing, arrowhead indicates original location of duct. Bar, 100 μm. (C) Following laser severing, the g1P projection continues to grow but the distance between the anterior tip of the projection and the original duct position remains roughly constant. The swelling of the projection in the anterior bulb is not unusual in older adults. Bar, 100 μm. (D) Merge of Nomarski differential interference contrast (NDIC) and GFP images for animal shown in C.

muscles (Figure 8). First, growth of glands may be dependent on their attachment to the pharyngeal lumen. For example, growth of the pharynx may place tension on the gland projection to stimulate growth; loss of this attachment by severing could result in a failure of the gland projection to grow or even in a retraction of the projection during subsequent growth of the pharynx. Thus, the length of the gland projection would remain constant or would shrink following surgery, with the distance between the duct and point of surgery increasing as the pharynx grows. The second possibility is that, following severing, the gland projection might fully regenerate, as occurs in *C. elegans* neurons following similar laser severing ("axotomy") (Yanik *et al.* 2004). Regeneration would only occur if the gland projection was able to penetrate past the pharyngeal muscles. Thus a third possibility is that, following severing, pharyngeal muscles would press in on the severed portion of the gland projection, ultimately preventing further growth of the cell into this region. However, the intact portion of the projection could continue to grow.

We found that, following laser surgery, gland projections maintained the distance between the distal end of the projection where severing occurred and the original site of the duct ($n = 9$). This is consistent with the third possibility described above, in which glands continue to grow, keeping pace with pharyngeal growth but do not regenerate past the point where they were severed. This result suggests that muscle and gland growth are counterbalanced: where the gland projection remains intact, the gland is able to continue growing in scale with the rest of the pharynx; where the gland projection has been eliminated as a result of severing, the pharyngeal muscles "close in" and prevent further invasion by the glands. While this result is consistent with a model in which glands and muscles exert pressure on one another, an alternate interpretation is that gland projections adhere to pharyngeal muscles along their length and that this adhesion stimulates gland growth, pulling it along as the muscle lengthen. We attempted to distinguish between these two interpretations by performing laser ablation of muscles in animals, to see whether glands grew into the area of ablated cells. While such laser treatment did appear to result in swelling of glands in the area of surgery (data not shown), the animals were badly damaged and did not survive long after surgery, preventing appropriate analysis.

Discussion

The long cellular projections of the pharyngeal glands extend to discrete points along the length of the pharynx, allowing the glands to secrete material into the pharyngeal lumen. At least one function of the glands is to secrete mucin-like PHAT proteins that line the pharyngeal lumen, and these secretions may aid in the passage of food along the pharynx (Smit *et al.* 2008). Complete coverage of the pharyngeal lumen by these secretions may thus be achieved in part by having multiple points of secretion along the length of the organ, at the sites of the gland ducts. Here we have investigated how the gland projections are maintained during development and growth of *C. elegans*. Following the establishment of these long cellular projections, their shape in subsequent growth and development is constrained by the surrounding pharyngeal muscles. Thus, the shape of the gland projections is not strictly an inherent property of the cell, but results instead from interactions between the glands and the organ environment in which they develop. Notably, in a variety of mutants with impaired pharyngeal muscles, gland projections become abnormally swollen and/or branched, apparently as a result of overgrowth that is not properly constrained by the pharyngeal muscles.

While we have tested multiple mutants affecting pharyngeal muscle integrity, the effects of these mutations on gland morphology may not occur via a single mechanism. For example, mutants in which pharyngeal elongation and hence muscle morphology is abnormal (such as *sma-1* and *let-502*) may result in gland hypertrophy through loss of one regulatory mechanism, while mutants affecting pharyngeal muscle ultrastructure and/or function (such as *tnt-4* and *unc-89*) may have a different effect on gland growth. Interestingly, our genetic screen identified other mutants with localized defects in the pharyngeal gland projections, but apparently normal pharynx morphology. Such mutants may specifically affect the ultrastructure of specific subsets of pharyngeal muscles, resulting in regional defects in gland projections. For example, the gland defects in *iv37* mutants may result from specific defects in the muscles of the anterior bulb (pm4 muscles), rather than some defect localized to a specific region of the gland projection.

One interesting problem faced by cells with long cellular projections, like the glands, is the issue of "scaling," *i.e.*, maintaining an appropriate length in relation to the rest of the organism during growth. How do the gland projections scale during growth of the pharynx? One simple expectation was that gland projections are anchored by the ducts at one end and by the cell bodies at the other end. In other systems, tension-induced growth may be responsible for scaling of long projections (Bray 1984). However, gland projections continue to grow following laser surgery that separates the gland projection from the duct. This result suggests that scaling of the gland projections does not require a single "anchor" like the duct. Instead, the gland projection may adhere to the pharyngeal muscles along its length, thus providing tension in response to muscle growth. Alternatively, the glands may neither adhere to the muscles nor require tension for growth, and may simply be opportunistic in their growth, held back largely by the force of the surrounding muscles. While we cannot currently distinguish between these models, the behavior of the glands in *sma-1* (and other) mutants suggests that gland projections are not subject to pulling forces, but rather push outwards, with the muscles normally functioning to constrain the projection and prevent overgrowth.

Establishment or maintenance of cell morphology by mechanical constraint from surrounding tissue is not unique to the pharyngeal glands. In many situations, cellular morphology is critically influenced by interactions with other cells and/or components of the ECM. For example, branching of mammalian salivary glands (to which the pharyngeal glands are likely related; Smit *et al.* 2008) depends on forces generated by surrounding tissue. Salivary gland branching is initiated by budding of the early gland, which begins as a sac-like ball of cells. This budding results not from intrinsic forces in the gland epithelia, but rather due to localized pressure from surrounding mesenchyme and ECM (Hsu and Yamada 2010). Regulation of mammary gland branching and growth also bears interesting similarities to the regulation of pharyngeal gland morphology. In mammary glands, new glandular branches are formed by growth and proliferation of lumenal epithelial cells, but this branching and growth is counterbalanced by the surrounding by myoepithelial cells. Growth of new branches occurs at sites where lumenal epithelia is not surrounded by myoepithelial cells. Growth is eventually blocked by the myoepithelial cells reestablishing coverage of the nascent lumenal branch, suggesting some form of growth constraint, much as growth of the pharyngeal glands appears to be constrained by surrounding myoepithelial cells (Ewald *et al.* 2008). It is interesting to note that some of the pharyngeal gland defects present as branching of the gland projection; one can imagine the development of more elaborate branched structures by alterations in local mechanical constraint. Mechanical forces are also thought to regulate growth in the case of "cell competition" in the *Drosophila* wing disc, in which slower growing clones of cells are outcompeted by faster growing neighbors, ultimately leading to apoptosis of the smaller clones, thereby ensuring uniform growth of the wing disc (Shraiman 2005). More generally, the shape of individual cells in an epithelial layer is a consequence of their interactions with neighbors and the resulting forces exerted by cells on one another (Gibson and Gibson 2009). A key difference in the case of the pharyngeal glands is that neither the glands nor the surrounding musculature are proliferative, and any growth of the tissue is strictly due to an increase in cell size rather than cell number. Thus, in this case, mechanical constraint by pharyngeal muscles acts solely to regulate expansion of the gland cells. How such mechanotransduction works at a molecular level in the glands is unclear, just as it is unclear whether or how glands are connected to neighboring muscles. Study of additional mutants from our screen, together with testing of candidate growth control genes, should provide insight into the underlying mechanism(s) that act to control pharyngeal gland growth and maintain the morphology of the long cellular projections.

Interestingly, the pharyngeal glands (also called esophageal glands) of other nematodes generally resemble those of *C. elegans*, with cell bodies in the posterior of the pharynx and long cellular extensions that reach to discrete points along the length of the pharynx (Chitwood and Chitwood 1950). In most cases, the dorsal gland (comparable to g1P) extends to near the end of the pharynx, while the subventral glands (comparable to g1A) extend roughly halfway along the length of the pharynx, though there are some exceptions with respect to both cell body position and length of projections. Notably, there is some diversity in the relative size of the gland projections, with some glands having relatively thin projections like those in *C. elegans* and others having projections that are roughly as wide as the cell body itself. Our results suggest that one way in which gland morphology can be affected through evolution is by alterations in the relative force exerted by the pharyngeal muscles on the gland projections. Thus, the variations in gland morphology among different nematode species may reflect differences in muscle structure or architecture as well as or instead of differences in the glands themselves.

Acknowledgments

The authors thank J. B. Rattner for assistance with TEM, Andy Fire for providing GFP vectors, and Paul Mains, Jim McGhee, Dave Hansen, and two anonymous reviewers, for helpful comments and advice. Some nematode strains used in this work were provided by the Caenorhabditis Genetics Center, which is funded by the National Institutes of Health's National Center for Research Resources. This work was supported by an operating grant from the Canadian Institutes of Health Research (to J.G.). J.G. is supported by Alberta Innovates–Health Solutions and the Canada Research Chairs (tier 2) programs.

Literature Cited

Albertson, D. G., and J. N. Thomson, 1976 The pharynx of *Caenorhabditis elegans*. Philos. Trans. R. Soc. Lond. B Biol. Sci. 275: 299–325.

Amin, M. Z., T. Bando, R. Ruksana, F. Anokye-Danso, Y. Takashima *et al.*, 2007 Tissue-specific interactions of TNI isoforms with other TN subunits and tropomyosins in C. elegans: the role of the C- and N-terminal extensions. Biochim. Biophys. Acta 1774: 456–465.

Amin, N. M., H. Shi, and J. Liu, 2010 The FoxF/FoxC factor LET-381 directly regulates both cell fate specification and cell differentiation in C. elegans mesoderm development. Development 137: 1451–1460.

Aspock, G., G. Ruvkun, and T. R. Burglin, 2003 The Caenorhabditis elegans ems class homeobox gene ceh-2 is required for M3 pharynx motoneuron function. Development 130: 3369–3378.

Avery, L., 1993 The genetics of feeding in *Caenorhabditis elegans*. Genetics 133: 897–917.

Benian, G. M., T. L. Tinley, X. Tang, and M. Borodovsky, 1996 The *Caenorhabditis elegans* gene *unc-89*, required for muscle M-line assembly, encodes a giant modular protein composed of Ig and signal transduction domains. J. Cell Biol. 132: 835–848.

Bray, D., 1984 Axonal growth in response to experimentally applied mechanical tension. Dev. Biol. 102: 379–389.

Brenner, S., 1974 The genetics of *Caenorhabditis elegans*. Genetics 77: 71–94.

Chisholm, A. D., and J. Hardin, 2005 Epidermal morphogenesis, WormBook, ed. The *C. elegans* Research Community, WormBook, doi/10.1895/wormbook.1.35.1, http://www.wormbook.org.

Chitwood, B. G., and M. B. Chitwood, 1950 *Introduction to Nematology*. University Park Press, Baltimore.

Davis, M. W., M. Hammarlund, T. Harrach, P. Hullett, S. Olsen *et al.*, 2005 Rapid single nucleotide polymorphism mapping in C. elegans. BMC Genomics 6: 118.

Dixon, S. J., and P. J. Roy, 2005 Muscle arm development in Caenorhabditis elegans. Development 132: 3079–3092.

Evans, T. C., 2006 Transformation and microinjection (April 6, 2006), *WormBook*, ed. The *C. elegans* Research Community, WormBook, doi/10.1895/wormbook.1.108.1, http://www.wormbook.org.

Ewald, A. J., A. Brenot, M. Duong, B. S. Chan, and Z. Werb, 2008 Collective epithelial migration and cell rearrangements drive mammary branching morphogenesis. Dev. Cell 14: 570–581.

Fay, D. S., X. Qiu, E. Large, C. P. Smith, S. Mango *et al.*, 2004 The coordinate regulation of pharyngeal development in C. elegans by lin-35/Rb, pha-1, and ubc-18. Dev. Biol. 271: 11–25.

Fire, A., S. Xu, M. K. Montgomery, S. A. Kostas, S. E. Driver *et al.*, 1998 Potent and specific genetic interference by double-stranded RNA in *Caenorhabditis elegans*. Nature 391: 806–811.

Franks, D. M., T. Izumikawa, H. Kitagawa, K. Sugahara, and P. G. Okkema, 2006 C. elegans pharyngeal morphogenesis requires both de novo synthesis of pyrimidines and synthesis of heparan sulfate proteoglycans. Dev. Biol. 296: 409–420.

Gally, C., F. Wissler, H. Zahreddine, S. Quintin, F. Landmann *et al.*, 2009 Myosin II regulation during C. elegans embryonic elongation: LET-502/ROCK, MRCK-1 and PAK-1, three kinases with different roles. Development 136: 3109–3119.

Garigan, D., A. L. Hsu, A. G. Fraser, R. S. Kamath, J. Ahringer *et al.*, 2002 Genetic analysis of tissue aging in *Caenorhabditis elegans*: a role for heat-shock factor and bacterial proliferation. Genetics 161: 1101–1112.

Gaudet, J., and S. E. Mango, 2002 Regulation of organogenesis by the Caenorhabditis elegans FoxA protein PHA-4. Science 295: 821–825.

Gibson, W. T., and M. C. Gibson, 2009 Cell topology, geometry, and morphogenesis in proliferating epithelia. Curr. Top. Dev. Biol. 89: 87–114.

Han, M., and P. W. Sternberg, 1990 *let-60*, a gene that specifies cell fates during *C. elegans* vulval induction, encodes a ras protein. Cell 63: 921–931.

Heiman, M. G., and S. Shaham, 2009 DEX-1 and DYF-7 establish sensory dendrite length by anchoring dendritic tips during cell migration. Cell 137: 344–355.

Hsu, J. C., and K. M. Yamada, 2010 Salivary gland branching morphogenesis–recent progress and future opportunities. Int. J. Oral Sci. 2: 117–126.

Kamath, R. S., A. G. Fraser, Y. Dong, G. Poulin, R. Durbin *et al.*, 2003 Systematic functional analysis of the Caenorhabditis elegans genome using RNAi. Nature 421: 220–221.

Kohara, Y., 2001a NEXTDB: The Nematode Expression Pattern Database. Kohara laboratory. Available from: http://nematode.lab.nig.ac.jp/. Accessed: August 2010.

Kohara, Y., 2001b Systematic analysis of gene expression of the C. elegans genome Tanpakushitsu Kakusan Koso 46: 2425–2431 (in Japanese).

Kormish, J. D., J. Gaudet, and J. D. McGhee, 2010 Development of the *C. elegans* digestive tract. Curr. Opin. Genet. Dev. 20: 346–354.

Kramer, J. M., R. P. French, E.-C. Park, and J. J. Johnson, 1990 The *Caenorhabditis elegans rol-6* gene, which interacts with the *sqt-1* collagen gene to determine organismal morphology, encodes a collagen. Mol. Cell. Biol. 10: 2081–2089.

Ma, P. C., M. A. Rould, H. Weintraub, and C. O. Pabo, 1994 Crystal structure of MyoD bHLH domain-DNA complex: perspectives on DNA recognition and implications for transcriptional activation. Cell 77: 451–459.

Maeda, I., Y. Kohara, M. Yamamoto, and A. Sugimoto, 2001 Large-scale analysis of gene function in Caenorhabditis elegans by high-throughput RNAi. Curr. Biol. 11: 171–176.

Mango, S. E., 2009 The molecular basis of organ formation: insights from the C. elegans foregut. Annu. Rev. Cell Dev. Biol. 25: 597–628.

Mani, K., and D. S. Fay, 2009 A mechanistic basis for the coordinated regulation of pharyngeal morphogenesis in Caenorhabditis elegans by LIN-35/Rb and UBC-18-ARI-1. PLoS Genet. 5: e1000510.

McGhee, J. D., T. Fukushige, M. W. Krause, S. E. Minnema, B. Goszczynski *et al.*, 2009 ELT-2 is the predominant transcription factor controlling differentiation and function of the C. elegans intestine, from embryo to adult. Dev. Biol. 327: 551–565.

McKeown, C., V. Praitis, and J. Austin, 1998 sma-1 encodes a betaH-spectrin homolog required for Caenorhabditis elegans morphogenesis. Development 125: 2087–2098.

McMahon, L., R. Legouis, J. L. Vonesch, and M. Labouesse, 2001 Assembly of C. elegans apical junctions involves positioning and compaction by LET-413 and protein aggregation by the MAGUK protein DLG-1. J. Cell Sci. 114: 2265–2277.

Mello, C. C., J. M. Kramer, D. Stinchcomb, and V. Ambros, 1991 Efficient gene transfer in *C. elegans*: extrachromosomal maintenance and integration of transforming sequences. EMBO J. 10: 3959–3970.

Mohler, W. A., J. S. Simske, E. M. Williams-Masson, J. D. Hardin, and J. G. White, 1998 Dynamics and ultrastructure of developmental cell fusions in the *Caenorhabditis elegans* hypodermis. Curr. Biol. 8: 1087–1090.

Morck, C., C. Axang, M. Goksor, and M. Pilon, 2006 Misexpression of acetylcholinesterases in the C. elegans pha-2 mutant accompanies ultrastructural defects in pharyngeal muscle cells. Dev. Biol. 297: 446–460.

Morck, C., C. Axang, and M. Pilon, 2003 A genetic analysis of axon guidance in the C. elegans pharynx. Dev. Biol. 260: 158–175.

Morck, C., M. Rauthan, F. Wagberg, and M. Pilon, 2004 pha-2 encodes the C. elegans ortholog of the homeodomain protein HEX and is required for the formation of the pharyngeal isthmus. Dev. Biol. 272: 403–418.

Norman, K. R., and D. G. Moerman, 2002 Alpha spectrin is essential for morphogenesis and body wall muscle formation in Caenorhabditis elegans. J. Cell Biol. 157: 665–677.

Parrish, J. Z., P. Xu, C. C. Kim, L. Y. Jan, and Y. N. Jan, 2009 The microRNA bantam functions in epithelial cells to regulate scaling growth of dendrite arbors in drosophila sensory neurons. Neuron 63: 788–802.

Pilon, M., 2008 Fishing lines, time-delayed guideposts, and other tricks used by developing pharyngeal neurons in Caenorhabditis elegans. Dev. Dyn. 237: 2073–2080.

Portereiko, M. F., and S. E. Mango, 2001 Early morphogenesis of the Caenorhabditis elegans pharynx. Dev. Biol. 233: 482–494.

Praitis, V., E. Ciccone, and J. Austin, 2005 SMA-1 spectrin has essential roles in epithelial cell sheet morphogenesis in C. elegans. Dev. Biol. 283: 157–170.

Priess, J. R., and D. I. Hirsh, 1986 *Caenorhabditis elegans* morphogenesis: the role of the cytoskeleton in elongation of the embryo. Dev. Biol. 117: 156–173.

Qiu, X., and D. S. Fay, 2006 ARI-1, an RBR family ubiquitin-ligase, functions with UBC-18 to regulate pharyngeal development in C. elegans. Dev. Biol. 291: 239–252.

Raharjo, I., and J. Gaudet, 2007 Gland-specific expression of *C. elegans hlh-6* requires the combinatorial action of three distinct promoter elements. Dev. Biol. 302: 295–308.

Rasband, W. S., 1997–2010 ImageJ. National Institutes of Health, Bethesda, Maryland, http://imagej.nih.gov/ij/.

Rasmussen, J. P., K. English, J. R. Tenlen, and J. R. Priess, 2008 Notch signaling and morphogenesis of single-cell tubes in the C. elegans digestive tract. Dev. Cell 14: 559–569.

Rogalski, T. M., B. D. Williams, G. P. Mullen, and D. G. Moerman, 1993 Products of the unc-52 gene in Caenorhabditis elegans are homologous to the core protein of the mammalian basement membrane heparan sulfate proteoglycan. Genes Dev. 7: 1471–1484.

Savage, C., P. Das, A. L. Finelli, S. R. Townsend, C. Sun *et al.*, 1996 *Caenorhabditis elegans genes sma-2*, *sma-3*, and *sma-4* define a conserved family of transforming growth factor-beta pathway components. Proc. Natl. Acad. Sci. USA 93: 790–794.

Shraiman, B. I., 2005 Mechanical feedback as a possible regulator of tissue growth. Proc. Natl. Acad. Sci. USA 102: 3318–3323.

Smit, R. B., R. Schnabel, and J. Gaudet, 2008 The HLH-6 transcription factor regulates C. elegans pharyngeal gland development and function. PLoS Genet. 4: e1000222.

Sulston, J. E., E. Schierenberg, J. G. White, and J. N. Thomson, 1983 The embryonic cell lineage of the nematode *Caenorhabditis elegans*. Dev. Biol. 100: 64–119.

Timmons, L., and A. Fire, 1998 Specific interference by ingested dsRNA. Nature 395: 854.

Waterston, R. H., J. N. Thomson, and S. Brenner, 1980 Mutants with altered muscle structure of Caenorhabditis elegans. Dev. Biol. 77: 271–302.

Wissmann, A., J. Ingles, J. D. McGhee, and P. E. Mains, 1997 Caenorhabditis elegans LET-502 is related to Rho-binding kinases and human myotonic dystrophy kinase and interacts genetically with a homolog of the regulatory subunit of smooth muscle myosin phosphatase to affect cell shape. Genes Dev. 11: 409–422.

Yanik, M. F., H. Cinar, H. N. Cinar, A. D. Chisholm, Y. Jin *et al.*, 2004 Neurosurgery: functional regeneration after laser axotomy. Nature 432: 822.

Communicating editor: K. Kemphues

GENETICS

Supporting Information
http://www.genetics.org/content/suppl/2011/08/25/genetics.111.132449.DC1

Cell Architecture: Surrounding Muscle Cells Shape Gland Cell Morphology in the *Caenorhabditis elegans* Pharynx

Wahyu Hendrati Raharjo, Vikas Ghai, Aidan Dineen, Michael Bastiani, and Jeb Gaudet

DOI: 10.1534/genetics.111.132449

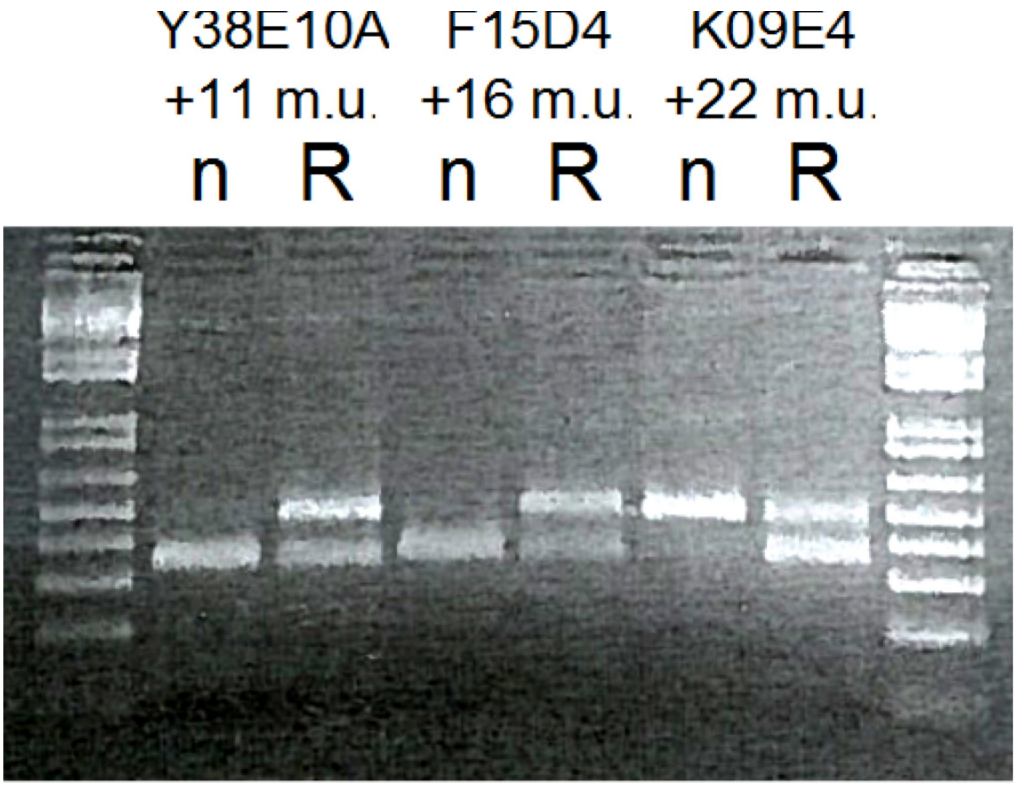

Figure S1 Suppression of recombination along the right arm of LG II in strain GD139 *ivIs12 [phat-1::YFP elt-2::GFP rol-6]*. BSA-SNP analysis shows no detectable recombination at three SNPs along the right arm of LG II. Progeny from +/*ivIs12* mothers collected in bulk are: 'n' = non-Roller, non-transgenic (+/+) and 'R' = Roller, transgenic (+/*ivIs12* and *ivIs12* homozygotes). At each SNP, non-Rollers show only the Hawaiian (CB4856) form of the SNP. A fourth SNP (Y6D1A at +4 m.u.) also shows only the Hawaiian form in non-transgenics (not shown).

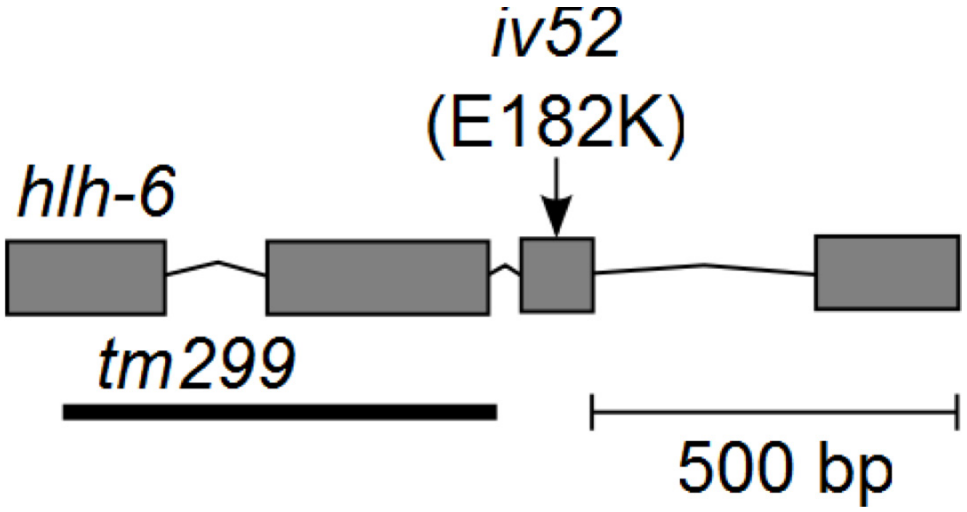

Figure S2 Diagram of *hlh-6* gene, indicating the previously described *tm299* deletion allele and the newly isolated missense mutation, *iv52*.

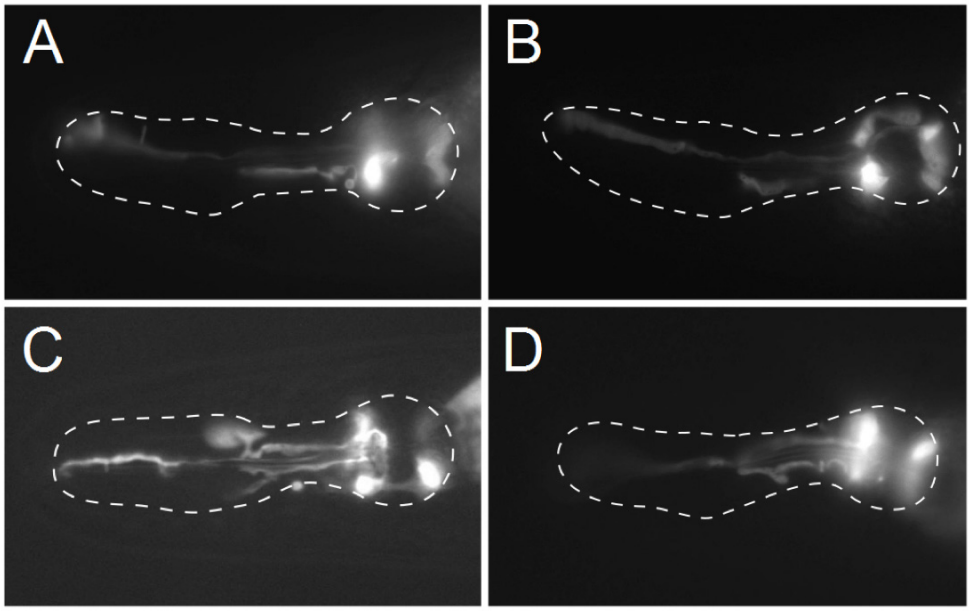

Figure S3 Additional examples of gland defects in *sma-1(iv38)* animals. **(A)** Branching of g1P visible in anterior pharynx, as well as swelling and blebbing of g1A projection. **(B)** Swelling of both g1P and g1A projections. **(C)** Extensive branching and swelling of all projections. **(D)** Branching and swelling of g1A projections; anterior g1P projection is out-of-plane.